


# EFFECTS OF PROPELLER FOULING ON THE HYDRODYNAMIC PERFORMANCE OF A MARINE PROPELLER

Ali Zinati 

Department of Maritime Engineering, Amirkabir University of Technology, Tehran, Islamic Republic of Iran

Mohammad Javad Ketabdari

Department of Maritime Engineering, Amirkabir University of Technology, Tehran, Islamic Republic of Iran

Hamid Zeraatgar 

Faculty of Marine Technology, Amirkabir University of Technology, Tehran, Islamic Republic of Iran

\* Corresponding author: hamidz@aut.ac.ir (Hamid Zeraatgar)

## ABSTRACT

*Propeller performance is typically considered under clean conditions, despite the fact that fouling is an inevitable phenomenon for propellers. The main objective of this study is to investigate the effects of roughness due to fouling on the performance of a propeller using a CFD simulation in conjunction with the roughness function model. A simulation of a clean propeller is verified for a five-blade propeller model using existing experimental results. A roughness function model is then suggested based on existing measured roughness data. The simulations are extended for the same propeller under varying severities of roughness. Initially, it is concluded that  $K_T$  and  $\eta_o$  gradually decrease with increasing fouling roughness, while  $K_Q$  increases, compared to smooth propeller. For instance, at  $J=1.2$  for medium calcareous fouling,  $K_T$  is reduced by about 26%,  $K_Q$  increases by about 7.0%, and  $\eta_o$  decreases by 30.9%. In addition, for the rough propeller, the extra power required is defined as the specific sea margin (SSM) to compensate for the power loss. A slight roughness causes a large decrease in  $\eta_o$ . A propeller painted with foul-release paint and an unpainted propeller are found to require 2.7% SSM and 57.8% SSM over four years of service, respectively. Finally, the use of foul-release paints for propeller painting is strongly advised.*

**Keywords:** Propeller performances, Blade roughness, Frictional resistance, CFD simulation, Fouling

## INTRODUCTION

Nowadays, shipping is a more important means of transportation compared to land and aviation. World globalisation has increased shipping traffic, transportation, and the capacities of goods transporters, which has increased fuel consumption as a result. Ships are a contributor to greenhouse gas (GHG) emissions [1], and in recent years, increasing pressure has been placed on the marine industry to decrease GHG emissions through regulatory legislation. IMO (International Maritime Organization) indicated that efficiency improvements could be achieved through operational [2] and technological methods, as these could increase overall performance and decrease fuel consumption

[3-10]. Temporary roughness, which refers to temporal changes in the hull and propeller surface roughness, is caused by fouling organisms during a period of service [8]. The increase in skin resistance due to fouling is responsible for a significant proportion of the total resistance, as a small amount of fouling can cause a significant increase in fuel consumption and air pollution.

The effects of roughness on hulls and propellers can be evaluated using the boundary layer similarity law or the CFD method. Both of these methods require a roughness function for the surface in question.

As mentioned at ITTC 2021 [11], there is a need to adopt or develop new methods to predict the roughness effects of marine biofouling and modern fouling-control coatings on

ship hydrodynamics and propeller performance. For this reason, ITTC 2021 recommended that the roughness function should be determined or developed by researchers for different surface conditions [11].

Several roughness function models have been proposed that are appropriate for different surface conditions. Some of these consider antifouling coatings such as the Townsin [12], Demirel [13], Vargas [14], and Grigson of Colebrook types [15]. One roughness function model proposed by Song [16] was appropriate for polished surfaces with sandpaper 60 and 80. Another roughness function model for surfaces covered with closely packed sand grain roughness was proposed by Cebeci [17]. The effects of biofilm can be predicted using the roughness function model of Farkas [18]. However, research on roughness function models is still needed, as indicated by ITTC 2021 [11] for the prediction of the roughness effects of marine biofouling.

The impacts of hard fouling and biofilm on the performance of ships using the roughness function proposed by Grigson were studied by Farkas et al. [19, 20]. The impact of inhomogeneous roughness distribution on the frictional resistance of a plate was considered using the roughness function model in conjunction with a longitudinal roughness position [21].

The roughness effects of fouling conditions on the performance of some propellers have been investigated using CFD simulations. Kellett et al. [22] investigated the effect of biofouling on a real four-blade ship propeller at the model scale using the roughness function approach. Owen et al. [23] calculated the performance of a PPTC propeller under different fouling conditions using a previously developed roughness function. Song et al. [24, 25] investigated the roughness effect of barnacles with varying sizes and coverage of a KP505 propeller using a roughness function of the Grigson type. The impact of biofilm on propeller performance was studied by Farkas et al. [26-28]. These studies have indicated that biofilms significantly decrease propeller performance, and should therefore be given due importance.

CFD-based hydrodynamic analysis has been extensively employed in many areas of research. However, the literature review above indicates that CFD cannot represent the complex geometry of a rough surface such as a propeller. ITTC 2021 [11] recommended employing either the similarity law or CFD simulations in conjunction with the roughness function model in order to include roughness effects. The main objective of this study is to investigate the effects of roughness on propeller performance through the use of CFD simulation with a roughness function model. In addition, an attempt is made to introduce a new roughness function model. To achieve these aims, a five-blade propeller model is considered. The clean propeller is simulated and compared to existing experimental results for validation, and the simulations are then extended to represent several severities of roughness for the same propeller using the verified simulation setup. The results are analysed, and the extra power required to compensate for the power loss of the roughed propeller is formulated and estimated. The effects of painting propellers

as a means to diminish the roughness are also considered. The novelty of this study is that it sheds light on the details of the propeller performance with respect to surface roughness and presents a new roughness function model.

## EFFECTS OF ROUGHNESS ON THE BOUNDARY LAYER

A turbulent boundary layer is assumed to consist of two regions: an inner area and an outer area. The flow in the inner area is affected by the surface roughness, whereas the flow in the outer area is independent of the surface conditions.

The velocity profile for smooth walls in the log-law region of a turbulent boundary layer can be defined as follows:

$$U^+ = \frac{1}{\kappa} \ln(y^+) + B \quad (1)$$

where  $y^+$  is the non-dimensional normal distance from the wall,  $\kappa$  is the von Karman constant, and  $B$  is the smooth wall log-law intercept.

Roughness leads to a decrease in the log-law velocity profile, and the downward shift of the velocity profile for rough walls is known as the roughness function,  $\Delta U^+$ . The log-law velocity profile for rough walls in the turbulent boundary layer is [25]:

$$U^+ = \frac{1}{\kappa} \ln(y^+) + B - \Delta U^+ \quad (2)$$

Various parameters can be used to define roughness, but the most frequently used is the roughness height,  $k_s$ . The dimensionless form of the roughness height is the roughness Reynolds number  $k_s^+$ , defined as  $k_s^+ = k_s U_\tau / \nu$ , where  $U_\tau$  is the friction velocity.

The most common method of solving for the turbulent boundary layer flow near the wall is to implement a wall function approach using an appropriate roughness function model.

## PROPULSION CHARACTERISTICS

For a propeller in open-water conditions, the thrust coefficient,  $K_T$ , torque coefficient,  $K_Q$ , and efficiency,  $\eta_O$ , are expressed in non-dimensional forms. When the propeller is fitted aft of the hull, the incoming flow is non-uniform, and the quasi-propulsive efficiency coefficient,  $\eta_D$ , is a function of the open-water efficiency,  $\eta_O$ , the relative rotative efficiency,  $\eta_R$ , and the hull efficiency,  $\eta_H$ , as follows:

$$\eta_D = \eta_O \eta_H \eta_R \quad (3)$$

## NUMERICAL SIMULATION

In this section, the governing equations are introduced, the roughness function is presented, and the numerical simulations of smooth and roughed propellers are explained.

### MATHEMATICAL FORMULATION

The governing equations in this context are those of mass and momentum conservation, which for compressible flows in the Cartesian coordinate system are as follows [23]:

$$\frac{\partial(\rho \bar{u}_i)}{\partial x_i} = 0 \quad (4)$$

$$\frac{\partial(\rho \bar{u}_i)}{\partial x_i} + \frac{\partial}{\partial x_i}(\rho \bar{u}_i \bar{u}_j + \rho \bar{u}_i \bar{u}_j') = -\frac{\partial \bar{p}}{\partial x_i} + \frac{\partial \bar{\tau}_{ij}}{\partial x_j} \quad (5)$$

where  $\rho$  is the density,  $\rho \bar{u}_i \bar{u}_j'$  is the Reynolds stress,  $\bar{u}_i$  is the averaged Cartesian component velocity, and  $\bar{p}$  is the mean pressure.  $\bar{\tau}_{ij}$  are the mean viscous stress tensor components, as follows:

$$\bar{\tau}_{ij} = \mu \left( \frac{\partial \bar{u}_i}{\partial x_j} + \frac{\partial \bar{u}_j}{\partial x_i} \right) \quad (6)$$

where  $\mu$  is the dynamic viscosity.

The Reynolds-averaged Navier-Stokes (RANS) method is employed to solve the governing equations using the commercial CFD software STAR-CCM+. The flow variables are discretised in space using second-order schemes, and the convection term of the turbulence is used as a first-order upwind scheme. The shear stress transport (SST)  $k-\omega$  turbulence model is applied to the complete RANS equations, as this combines the advantages of the  $k-\omega$  and  $k-\epsilon$  turbulence models. In this model, the  $k-\omega$  formulation is applied to the inner part of the boundary layer, and the  $k-\epsilon$  formulation to the free stream, which gives better predictions of the flow separation and adverse pressure gradients. To achieve reliable results, an appropriate choice of grids is crucial.

Physical modeling of the roughness geometry is not practical in CFD, due to its complexity. The wall-function approach is therefore applied to solve the flow equations near the wall, rather than using turbulence-model equations up to the wall.

### PROPOSED ROUGHNESS FUNCTION

In general, roughness functions are obtained experimentally, since there is no universal roughness function model for all kinds of rough surfaces. It should be noted that

the impact of roughness on  $\Delta U^+$  depends on the type and coverage of the roughness.

In this study, the roughness parameters measured by Schultz and Flack [29] are used to develop a new roughness function model. The proposed model is fitted to the roughness function values reported by Schultz and Flack [29]. One advantage of our roughness function model is that it can be applied to all types of fouled surfaces and typical antifouling coatings. The values of the sand grain roughness height and other relevant data are shown in Table 1 for a range of surface conditions.

Tab. 1. Representative coating and fouling conditions [23]

Description of condition	NSTM rating*	$k_s$ ( $\mu\text{m}$ )	$R_{iso}$ ( $\mu\text{m}$ )
Hydraulically smooth surface	0.	0	0
Typical as applied AF coating	0	30	150
Deteriorated coating or light slime	10–20	100	300
Heavy slime	30	300	600
Small calcareous fouling or weed	40–60	1,000	1,000
Medium calcareous fouling	70–80	3,000	3,000
Heavy calcareous fouling	90–100	10,000	10,000

\* NSTM (2002): Naval Ships' Technical Manual

The proposed roughness function model is as follows:

$$\Delta U^+ = \begin{cases} 0 & k_s^+ \leq 2.5 \\ \frac{1}{\kappa} \ln(0.2667 k_s^+) \sin\left[\frac{\pi}{2} \frac{\log(k_s^+/2.5)}{\log(10)}\right] & 2.5 < k_s^+ < 25 \\ \frac{1}{\kappa} \ln(0.2667 k_s^+) & k_s^+ \geq 25 \end{cases} \quad (7)$$

A brief explanation of the development of this roughness function model is presented in Appendix A.

Fig. 1 shows a schematic representation of the proposed roughness function model in Eq. (7), and compares it with the measurements of Schultz and Flack [29]. Good agreement is observed between the two.

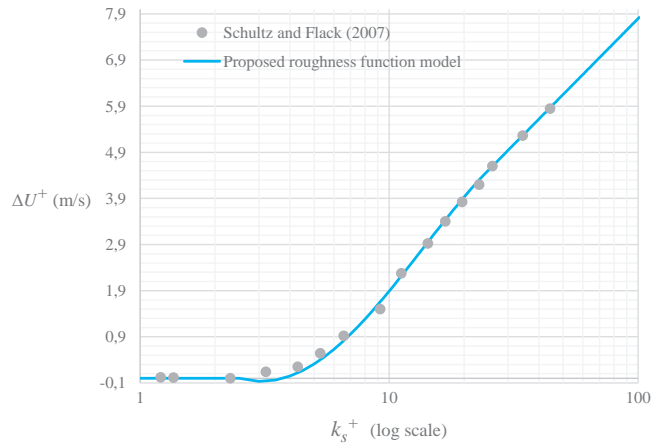


Fig. 1. Comparison of the proposed roughness function model with the values reported by Schultz and Flack [29]

The proposed roughness function model has a similar form to the built-in wall function of STAR-CCM+, and is employed as the wall function of STAR-CCM+. The proposed model is introduced to the CFD simulation setup via the coefficients  $B = 0$ ,  $C = 0.2667$ ,  $R^+_{smooth} = 2.5$ , and  $R^+_{rough} = 25$  (Eq. (7)), to replace the STAR-CCM+ coefficients  $B = 0$ ,  $C = 0.253$ ,  $R^+_{smooth} = 2.25$ , and  $R^+_{rough} = 90$ . Hence, the mathematical formulation and flow calculations around the rough propeller are the same as for the smooth propeller except for the roughness function model.

## PROPELLER GEOMETRY

The VP1304 propeller has often been used for computational case studies, and was selected here for analysis. It is a five-blade right-handed propeller model with a diameter of 250 mm (Fig. 2). Specifications of the propeller are shown in Table 2 [30].

Tab. 2. Specifications of the VP1304 propeller

Parameter	Symbol	Value	Units
Number of blades	$Z$	5	-
Diameter	$D$	0.250	m
Area ratio	$A_E/A_0$	0.779	-
Pitch ratio at 0.7 R	$P_{0.7}/D$	1.635	-
Chord length at 0.7 R	$C_{0.7}$	0.104	m
Hub ratio	$d_h/D$	0.3	-
Rotation rate	$n$	15	rps
Advance coefficient	$J$	0.6–1.2	-
Inflow speed	$V_A$	adjust	m/s

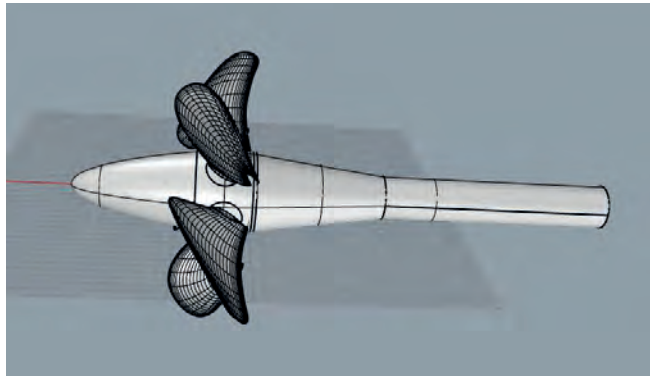


Fig. 2. Propeller geometry

## COMPUTATIONAL DOMAIN AND BOUNDARY CONDITIONS

The computational domain is depicted in Fig. 3, where the length and diameter of the domain for the open-water simulations are  $9D$  and  $4D$ , respectively. The inlet is located at a distance  $2D$  upstream, and the outlet is located at a distance  $7D$  downstream, to avoid any reflections and to ensure a uniform inflow. The top and bottom boundary distances

are  $2D$ . The computational domain consists of two parts: the inner region, which rotates with the propeller, and the outer part, which is fixed.

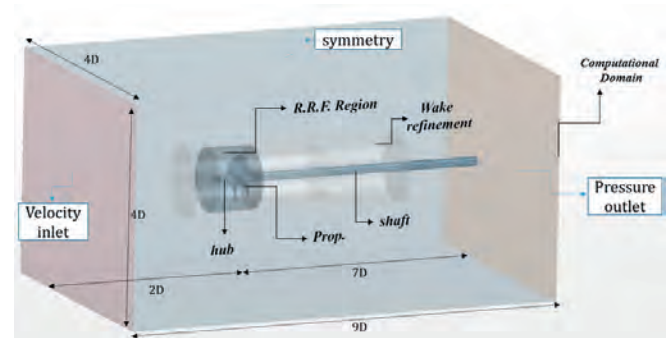


Fig. 3. Dimensions of the computational domain

Appropriate boundary conditions need to be applied to ensure accurate simulations. In this study, we set the velocity inflow for the inlet and the pressure boundary conditions for the outlet. The outer walls - are set to the slip wall condition, while a no-slip rough wall condition -is applied to the propeller, shaft, and hub, to represent rough surfaces. The water density and kinematic viscosity are  $998.67 \text{ kg/m}^3$  and  $1.070 \times 10^{-6} \text{ m}^2/\text{s}$ , respectively. The boundary conditions are summarised in Table 4 and Fig. 3.

Tab. 3. Boundary conditions

Region	Boundary	Type
Fixed parts	Inflow	Velocity inlet
	Outflow	Pressure outlet
	Shaft	No-slip condition
	Outer walls	Slip condition
Rotating parts	Hub	No-slip condition
	Blades	No-slip condition
	Interface	Nearest cell interpolation

## GRID GENERATION

In order to achieve reliable results, the generation of appropriate grids is crucial. The rotating reference frame (RRF) method is adopted for the propeller simulations in this study. Since RRF does not require a complicated mesh motion and a steady-state solver can be used, it is simpler and computationally cheaper than unsteady approaches. In this approach, the domain remains stationary, with an assigned frame of reference rotating about an axis in the global coordinate system. Fig. 4 depicts the structured and unstructured grids, and Fig. 5 shows the propeller surface grids. The outer cylinder is meshed with coarse grids, and the inner cylinder with fine ones. The distance of the first cell from the wall,  $y^+$ , is given in Fig. 6.



## RESULTS

This section presents the CFD results for the propeller. The computational results are first compared with open-water experimental results for a smooth propeller, for validation purposes. The simulation procedure is then applied to a range of fouling conditions to investigate the effects of fouling roughness on the open-water performance. Finally, the required extra power is introduced and estimated in terms of the *specific sea margin, SSM*, for the power loss of the roughened propeller. Values of the SSM are obtained for roughened and painted propellers.

### MESH SENSITIVITY AND VERIFICATION STUDY

A mesh sensitivity study is carried out to investigate the thrust coefficient for coarse to fine grids. Fig. 7 shows the uniform convergence of mesh sizes, and it can be seen that there are no signs of divergence or oscillation. The grid sensitivity is tested by estimating the numerical uncertainty. The grid convergence index (GCI) with the Richardson extrapolation [31] is employed to calculate the discretisation error, and a mesh refinement factor  $r = \sqrt{2}$  of is chosen.

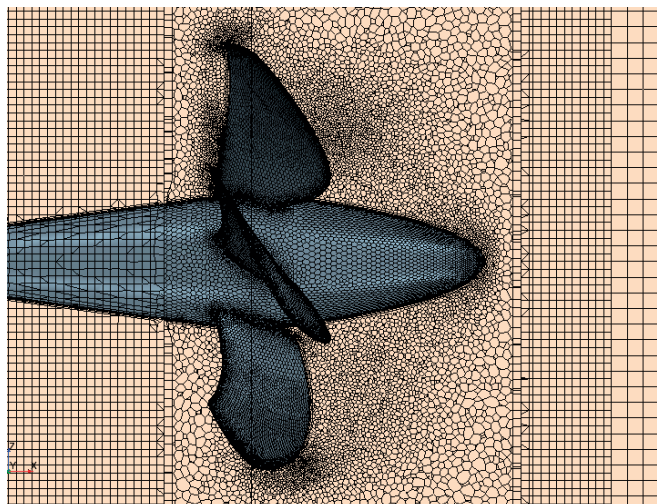


Fig. 4. Domain grids

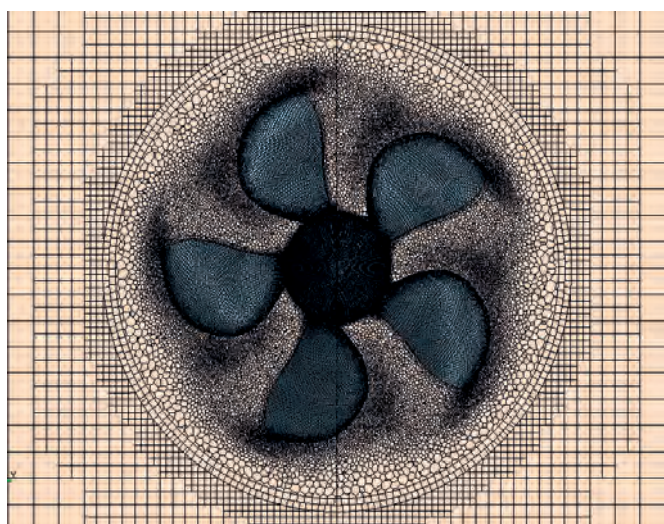


Fig. 5. Propeller surface grids

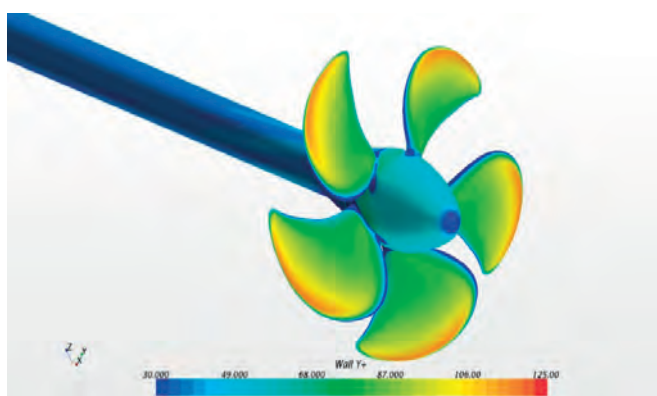


Fig. 6. Distance of the first cell from the wall,  $y^+$

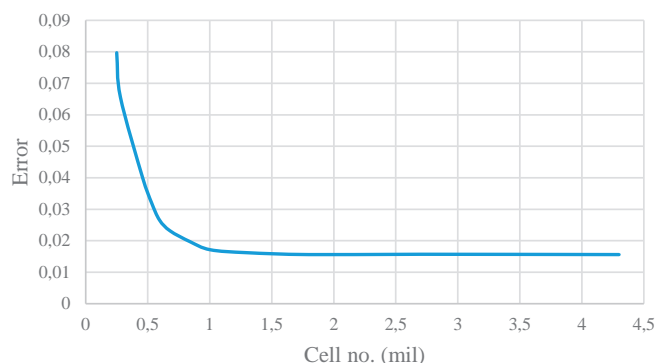


Fig. 7. Grid convergence results for  $K_t$

he uncertainty is obtained using the following equations:

$$\begin{aligned} \varepsilon_{21} &= \phi_2 - \phi_1 \\ \varepsilon_{32} &= \phi_3 - \phi_2 \end{aligned} \quad (8)$$

where the subscripts 1, 2, or 3 represent the numbers assigned to fine, medium, and coarse grids, respectively. is the function under consideration, which in this case is  $K_t$  or  $K_Q$ .

$$s = \text{sign} \left( \frac{\varepsilon_{32}}{\varepsilon_{21}} \right) \quad (9)$$

$$p_a = \frac{1}{\ln(r_{21})} \left| \ln \left| \left( \frac{\varepsilon_{32}}{\varepsilon_{21}} \right) \right| + q(p_a) \right| \quad (10)$$

$$q(p_a) = \ln \left[ \frac{r_{21}^{p_a} - s}{r_{21}^{p_a} - s} \right] \quad (11)$$

The extrapolated values are calculated as follows:

$$\phi_{ext}^{21} = \frac{(r_{21}^p \phi_1 - \phi_2)}{(r_{21}^p - 1)} \quad (12)$$

The approximate and extrapolated relative errors are obtained as:

$$e_a^{21} = \left| \frac{\phi_1 - \phi_2}{\phi_1} \right| \quad (13)$$

$$e_{ext}^{21} = \left| \frac{\phi_{ext}^{12} - \phi_1}{\phi_{ext}^{12}} \right| \quad (14)$$

The fine GCI is computed as:

$$GCI_{fine}^{21} = \frac{1.25 e_a^{21}}{r_{21}^p - 1} \quad (15)$$

where  $s, p_a, q(p_a), \Phi_{ext}^{21}, ea^{21}, e_{ext}^{21}$  are intermediate parameters.

The GCI is also calculated for  $K_T$  and  $K_Q$ . Values for the numerical uncertainty of 2.81% and 2.40% are obtained for the discretisation errors of  $K_T$  and  $K_Q$ , respectively. The required data and details of the GCI are presented in Table 4.

Tab. 4. Uncertainty calculations for  $K_T$  and  $K_Q$

	$K_T$	$K_Q$
$r_{21}$	$\sqrt{2}$	$\sqrt{2}$
$r_{32}$	$\sqrt{2}$	$\sqrt{2}$
$\phi_1$	0.50560	0.11744
$\phi_2$	0.50304	0.11718
$\phi_3$	0.50095	0.11689
$\epsilon_{21}$	-0.00256	-0.00026
$\epsilon_{32}$	-0.00209	-0.00029
$p_a$	0.58528	0.31508
$\phi_{ext}^{21}$	0.51698	0.11969
$e_a^{21}$	0.50%	0.22%
$e_{ext}^{21}$	2.20%	1.88%
$GCI_{fine}^{21}$	2.81%	2.39%

## VALIDATION OF THE SIMULATIONS

The open-water simulation results are compared with the results of experiments performed by Barkmann et al. [32] at a speed  $n = 15$  rps for the smooth propeller. The results for advance coefficients of  $J = 0.6-1.2$  are shown in Table 5.

Tab. 5. Experimental and simulation results for the open-water smooth propeller

$J$	Open-water test results [32]			Open-water CFD results		
	$K_T$	$K_Q$	$\eta_o$	$K_T$	$K_Q$	$\eta_o$
0.6	0.6288	1.3964	0.4300	0.5961	1.3593	0.4188
0.8	0.5100	1.1780	0.5512	0.5056	1.1744	0.5481
1.0	0.3994	0.9749	0.6520	0.4008	0.9993	0.6383
1.2	0.2949	0.7760	0.7258	0.3007	0.7855	0.7311

Fig. 8 shows both the numerical and experimental results for the smooth propeller. In general, good agreement between numerical and experimental results is achieved; a 5% discrepancy in  $K_T$  is the largest error observed for advance coefficients in the range 0.6-1.2.

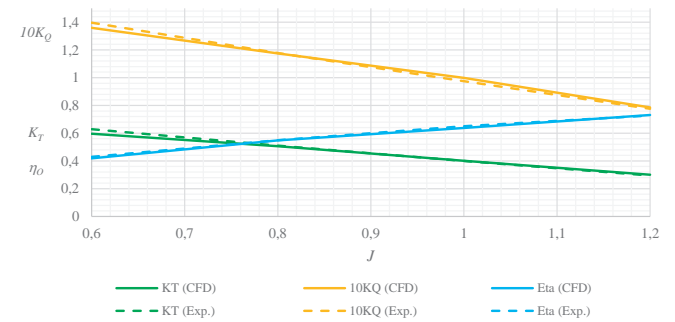


Fig. 8. Experimental [32] and CFD simulation results (current study) for a VP1304 propeller under smooth open-water conditions

The velocity contour at the surface of the propeller is shown in Fig. 9.

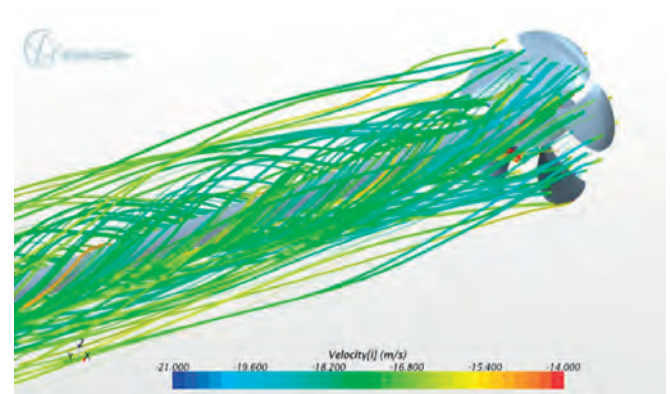


Fig. 9. Velocity contour

## EFFECT OF FOULING ON THE OPEN-WATER PERFORMANCE OF THE PROPELLER

In the following, the sand-grain roughness heights are used to represent the fouling conditions (Table 1). The results for the propeller performance at a speed of  $n = 15$  rps and values of  $J = 0.6-1.2$  are presented for different fouling conditions in Table 6 and Fig. 10, and are compared with the results for the smooth propeller.

It can be seen that  $K_T$  and  $\eta_o$  gradually decrease with increasing fouling roughness, while  $K_Q$  increases. For a value of  $J = 1.2$  for medium calcareous fouling,  $\eta_o$  is reduced by about 26% and  $K_Q$  increases by about 7.0% with respect to the smooth propeller. Consequently, a 30.9% decrease in  $\eta_o$  is observed. The effects of medium and heavy calcareous fouling on the open-water performance of the considered propeller are almost the same. The reason for this may be related to the relative height of the roughness and the sub-layer thickness.

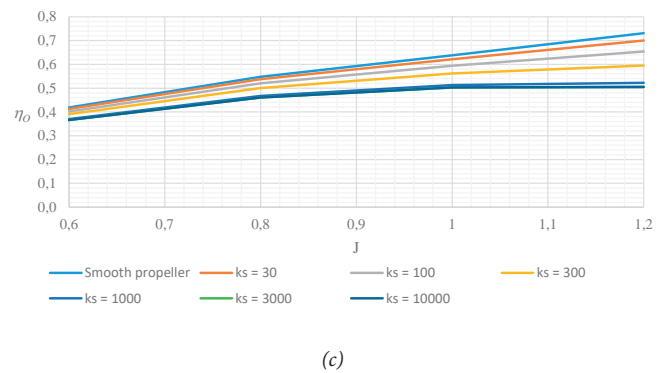
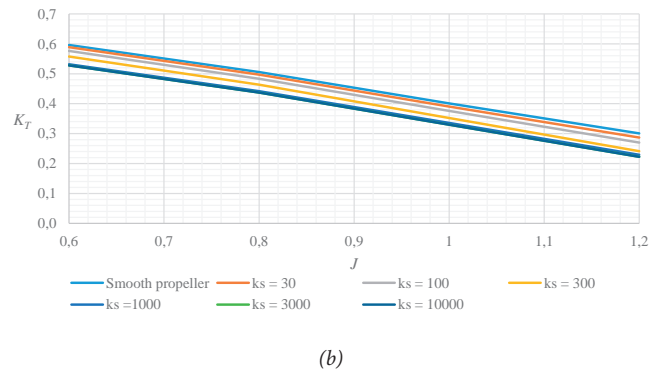
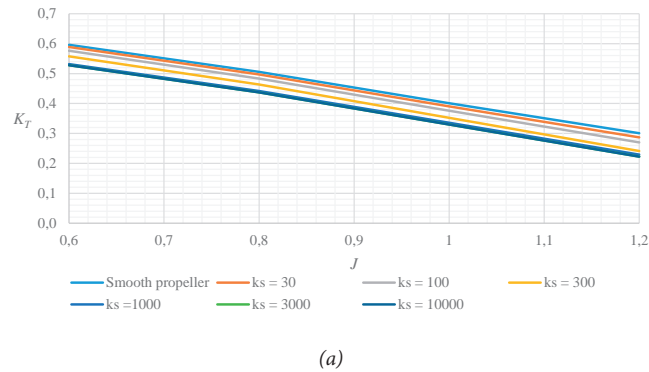


Fig. 10. Results for (a) the propeller thrust coefficient, (b) the torque coefficient, and (c) the efficiency for a range of surface conditions

To enable us to consider the roughness effect alone, Fig. 11(a) depicts  $K_T$  as a function of  $k_s$ . The slope of  $K_T$  versus  $k_s$  indicates that there is a large decline up to  $k_s = 500 \mu\text{m}$  over the whole range of  $J$ . It can be observed that  $K_T$  rapidly decreases as  $k_s$  increases up to  $k_s = 1000 \mu\text{m}$ ; for  $k_s$  in the range  $1000-3000 \mu\text{m}$ , a marginal decrease of  $K_T$  is observed, while  $K_T$  tends to a constant for  $k_s$  greater than  $3000 \mu\text{m}$ .

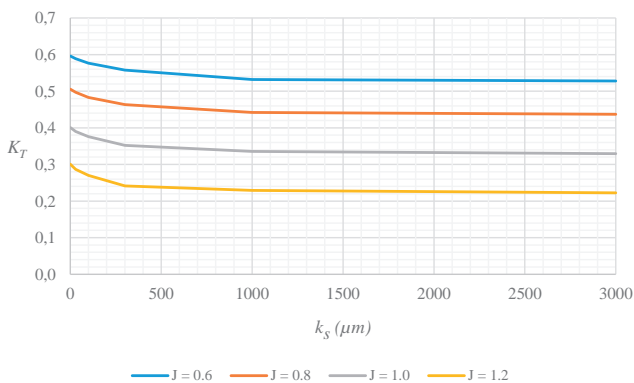
When  $\eta_o$  is plotted as a function of  $k_s$ , it shows the same tendency as  $K_T$ , as discussed above (Fig. 11(c)).

Fig. 11(b) shows  $K_Q$  as a function of  $k_s$ . It can be seen that  $K_Q$  increases with  $k_s$  up to a value of  $k_s = 1000 \mu\text{m}$ . For  $k_s$  in the range  $1000-3000 \mu\text{m}$ , a marginal increase in  $K_Q$  is observed, and  $K_Q$  is constant for  $k_s$  larger than  $3000 \mu\text{m}$ .

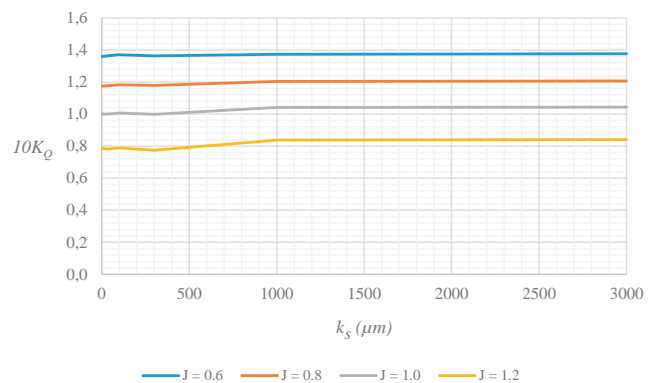
The slopes for  $K_T$ ,  $K_Q$ , and  $\eta_o$  versus  $k_s$  are larger at a value of  $J = 1.2$  than  $J = 0.6$ . Fig. 11(c) shows that for a higher value of  $J$ , there is a more significant reduction in  $\eta_o$ . Figs. 10(c) and 11(c) also show that a slight increase in roughness leads to a large decrease in the value of  $\eta_o$  for the propeller. This is conclusive evidence that the initial roughness up to small calcareous fouling has crucial effect. This finding supports those of studies by Song et al. [25], Farkas et al. [28], and Owen et al. [23], among others. Therefore, the importance of the initial roughness on the propeller performance is emphasised, and propeller painting is recommended as a solution. In other words, the rate of required power will increase as the roughness increases. The propeller roughness arises from the accumulation of fouling as a function of the time operating at sea, meaning that a large drop in propeller performance is expected in the early stages of operation.

Tab. 6. Computed open-water characteristics under different fouling conditions

Propeller surface/fouling condition	J	$K_T$	$\Delta K_T(\%)$	$10K_Q$	$\Delta K_Q(\%)$	$\eta_O$	$\Delta \eta_O(\%)$
Smooth propeller	0.6	0.5961	0	1.3593	0	0.4188	0
	0.8	0.5056	0	1.1744	0	0.5481	0
	1.0	0.4008	0	0.9993	0	0.6383	0
	1.2	0.3007	0	0.7855	0	0.7311	0
$k_s = 30 \mu m$	0.6	0.5889	-1.21	1.3630	0.27	0.4126	-1.48
	0.8	0.4969	-1.71	1.1764	0.17	0.5378	-1.88
	1.0	0.3901	-2.66	0.9992	-0.01	0.6214	-2.65
	1.2	0.2868	-4.62	0.7822	-0.42	0.7003	-4.21
$k_s = 100 \mu m$	0.6	0.5763	-3.33	1.3699	0.78	0.4017	-4.07
	0.8	0.4832	-4.42	1.1825	0.69	0.5203	-5.07
	1.0	0.3757	-6.27	1.0063	0.70	0.5942	-6.92
	1.2	0.2700	-10.20	0.7884	0.37	0.6541	-10.53
$k_s = 300 \mu m$	0.6	0.5576	-6.47	1.3627	0.25	0.3907	-6.70
	0.8	0.4637	-8.28	1.1789	0.38	0.5008	-8.63
	1.0	0.3523	-12.10	0.9984	-0.10	0.5616	-12.01
	1.2	0.2412	-19.78	0.7742	-1.44	0.5951	-18.60
$k_s = 1,000 \mu m$	0.6	0.5317	-10.81	1.3725	0.97	0.3699	-11.66
	0.8	0.4419	-12.60	1.2042	2.54	0.4672	-14.77
	1.0	0.3553	-16.33	1.0410	4.17	0.5127	-19.68
	1.2	0.2292	-23.77	0.8380	6.67	0.5224	-28.54
$k_s = 3,000 \mu m$	0.6	0.5279	-11.44	1.3764	1.26	0.3663	-12.54
	0.8	0.4370	-13.57	1.2067	2.75	0.4611	-15.88
	1.0	0.3295	-17.80	1.0432	4.39	0.5026	-21.26
	1.2	0.2225	-26.02	0.8408	7.04	0.5053	-30.89
$k_s = 10,000 \mu m$	0.6	0.5279	-11.44	1.3764	1.26	0.3663	-12.54
	0.8	0.4370	-13.57	1.2067	2.75	0.4611	-15.88
	1.0	0.3295	-17.80	1.0432	4.39	0.5026	-21.26
	1.2	0.2225	-26.02	0.8408	7.04	0.5053	-30.89



(a)



(b)



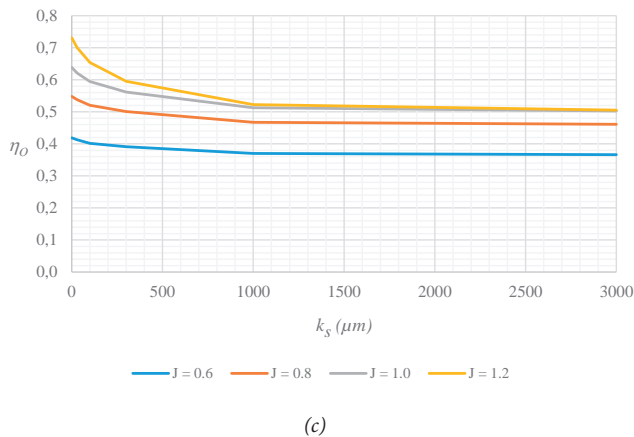


Fig. 11. Results for propeller performance: graphs of (a) thrust coefficient, (b) torque coefficient, and (c) efficiency versus roughness height

## VALIDATION OF THE ROUGHED PROPELLER SIMULATIONS

The literature does not contain a description of a rough propeller and a corresponding smooth propeller as reference that would enable a validation study, and it is therefore not possible to run a validation study on the rough propeller. Although two papers have been published by Owen et al. [23] and Song et al. [25] that deal with rough and smooth propellers, with two different roughness function models, insufficient data are publicly available to repeat these simulations.

It can be seen that for the same roughness conditions, the results of both this study and prior works indicate a significant change in the hydrodynamic performance of the propeller. For example, Owen et al. [23] reported maximum changes in  $K_T$ ,  $K_Q$ , and  $\eta_o$  of  $-25.5\%$ ,  $+6.9\%$ , and  $-30.3\%$  for  $k_s = 3,000 \mu\text{m}$ . The results of the current study predict changes in  $K_T$ ,  $K_Q$ , and  $\eta_o$  of  $-26.0\%$ ,  $+7.0\%$ , and  $-30.1\%$  for  $k_s = 3,000 \mu\text{m}$ .

On this basis, it can be seen that the changes in propeller performance calculated in the current study are qualitatively similar to those of other research.

## EFFECT OF PROPELLER PAINTING ON ENGINE BRAKE POWER

Our results indicate the importance of surface conditions on fuel consumption, and hence greenhouse gas emissions, which could be reduced by cleaning and appropriate propeller painting.

At the design stage, engine power is evaluated based on the assumption of smooth propeller conditions; however, a propeller will become rough, and the ship speed is consequently reduced. To maintain the speed calculated for the case of a clean propeller, one solution is to paint the propeller to keep its roughness below a certain level.

## Roughness height for painted propellers

The roughness of a painted propeller over a period of operation can be considered as the summation of the roughness of the painted surface ( $k_{s1}$ ) and the accumulation of fouling over a certain service time ( $k_{s2}$ ).

A value of  $k_{s1} = 0.17R_a$  can be used for painted propellers, according to Schultz [33] (Table 8). It should be noted that in this study, we use the roughness height of Schultz [33] but not the corresponding roughness function model.

Tab. 7. Annual roughness increments [34]

Coating type	Annual roughness increment $Rt_{50}$ ( $\mu\text{m}/\text{year}$ )
Traditional AF coating	40–60
Self-polishing coating, SPC	10–30
Foul-release paints, FR	5–15

The final roughness of the painted propeller is shown in Table 8 for three types of paint after four years of service.

Tab. 8. Final roughness of a painted propeller after four years of service

Paint type	Paint roughness $k_{s1}$ ( $\mu\text{m}$ )	Roughness due to fouling after four years based on Table 1		Final roughness $k_s$ ( $\mu\text{m}$ )
		$R_{150}$ ( $\mu\text{m}$ )	$k_{s2}$ ( $\mu\text{m}$ )	
Traditional AF coating	$k_s = 30$	$4 \times 50 = 200$	53	83
Self-polishing paints, SPC	$k_s = 0.17R_a = 3.4$	$4 \times 20 = 80$	16	19.4
Foul-release paints, FR	$k_s = 0.17R_a = 2.4$	$4 \times 10 = 40$	8	10.4
Note: In general, $R_a$ is about $20 \mu\text{m}$ for SPC and about $14 \mu\text{m}$ for FR paints [33]				

## Power estimation for fouled propellers

The ship hull is assumed to be clean, and only the propeller is fouled. Under these conditions, the power of the fouled propeller is derived based on the power for a clean propeller at the ship service speed,  $V_s$ . For a fouled propeller, the required torque,  $Q_p$ , increases for a given delivered power,  $P_D$ , which leads to a decrease in the propeller speed,  $n$ , and hence the ship speed,  $V_s$ . To maintain the ship speed calculated for the clean propeller condition, the engine power must be increased (referred to here as  $P_{Bf}$ ). The clean propeller scenario is considered here as a benchmark to estimate the extra power for the fouled propeller that leads to an estimate of SSM. The value of  $P_B$  for a clean propeller is calculated as follows:

$$P_B = \frac{P_E}{\eta_o \eta_H \eta_R \eta_m} = \frac{R_T V_s}{\eta_o \eta_H \eta_R \eta_m} \quad (16)$$

where  $R_T$  is total hull resistance, and  $\eta_m$  is the mechanical efficiency.

Assuming the same hull efficiency, mechanical efficiency and relative rotative efficiency for the clean and fouled

propellers,  $P_{Bf}$  for the fouled propeller can be estimated as follows:

$$P_{Bf} = \frac{P_E}{\eta_{Of}\eta_H\eta_R\eta_m} = \frac{R_T V_s}{\eta_{Of}\eta_H\eta_R\eta_m} \quad (17)$$

where  $\eta_o$  is the open-water efficiency of the fouled propeller.

For the fouled propeller,  $R_T$  and  $\eta_m$ , are the same as for the clean propeller. Based on the assumption that  $\eta_H$  and  $\eta_R$  are not significantly changed due to the propeller roughness,  $P_{Bf}$  is estimated as follows:

$$P_{Bf} = P_B \frac{\eta_o}{\eta_{of}} \quad (18)$$

### Specific sea margin

Sea margin is defined as the extra power required due to the sea state in comparison with still water, as well as a roughed hull in comparison with smooth hull conditions. To define the propeller roughness effect on engine power, we define the 'specific sea margin' (SSM) as the extra power required to maintain the ship speed in the case of a roughed propeller compared to a smooth propeller.

The SSM is estimated as follows:

$$SSM = \frac{P_{Bf} - P_B}{P_B} \times 100 = \left(\frac{P_{Bf}}{P_B} - 1\right) \times 100 = \left(\frac{\eta_o}{\eta_{of}} - 1\right) \times 100 \quad (19)$$

The justification of this formula SSM is examined and compared with  $\Delta P_s$  reported by Song et al. [25]. The concepts of SSM and  $\Delta P_s$  are similar, which is why these two different methods show good agreement.

### Specific sea margin for painted propellers

The performance of a propeller becomes worse with the fouling severity, as shown in Table 6. This table also shows that the performance of a propeller coated with antifouling paint is considerably better than that of a fouled propeller. The effects of fouled painted propellers are examined based on the propeller power, and SSM values for a propeller coated using three types of paint, after four years of service (becoming fouled), are considered. For the sake of simplicity, only the open-water efficiency is considered when predicting the extra power in terms of the SSM, and the effects of the other parameters such as  $\eta_H$ ,  $\eta_R$ , etc. are disregarded.

The final roughness height,  $k_s$ , for each type of paint after four years of service is determined as shown in Table 8. The efficiency of a roughed propeller,  $\eta_{op}$  is interpolated from Table 6 based on the final roughness height, and the SSM is calculated using Eq. (19). These data are presented in Table 9. It is worth mentioning that the first two cases represent fouled unpainted propellers, and the remainder are fouled painted propellers. At a given ship speed for a clean propeller, the SSM is calculated as 57.8%, 31.9%, 15.9%, 4.8%, and 2.7% for small

calcareous fouling, heavy slime fouling, antifouling paint, self-polishing paint, and foul-release paint, respectively. It can be seen that the painting of the propeller is extremely effective; for instance, the difference between SSM values of 57.8% and 2.7% is huge in terms of fuel consumption and gas emissions. Painting of propellers is therefore strongly advised, using foul-release paint.

Tab. 9. Comparison of SSM values for fouled unpainted and fouled painted propellers

Case	Propeller surface condition	$k_s$ ( $\mu\text{m}$ )	$\eta_{of}$ OR $\eta_o$	SSM (%)
1	Small calcareous fouling or weed	1000	0.4634	57.8
2	Heavy slime	300	0.5544	31.9
3	AF paintings	83	0.6310	15.9
4	Self-polishing coatings, SPC	19.4	0.6974	4.8
5	Foul-release paints, FR	10.38	0.7116	2.7
	Clean propeller ( $J=1.2$ )	0	0.7311	0

## CONCLUSION

The main goal of this study is to consider the effects of the roughness of a propeller on its performance using the CFD method. A five-blade propeller model is selected for the calculations, and a simulation of a clean propeller is verified. A new roughness function model is suggested based on existing measured roughness data. The simulations are extended to represent the same propeller under several roughness conditions, and the following conclusions could be drawn:

- A comparison of roughed and smooth propellers shows that  $K_T$  and  $\eta_o$  gradually decrease with increasing roughness up to  $k_s = 3,000 \mu\text{m}$ , while  $K_Q$  increases up to  $k_s = 3,000 \mu\text{m}$ . For instance, at  $J = 1.2$  for medium calcareous fouling,  $K_T$  reduces by about 26%,  $K_Q$  increases by about 7.0%, and  $\eta_o$  decreases by 30.9%.
- The effects of medium and heavy calcareous fouling on the open-water performance of the propeller are found to be almost the same.
- Graphs of  $K_T$ ,  $K_Q$ , and  $\eta_o$  versus  $k_s$  have larger slopes at  $J = 1.2$  than  $J = 0.6$ . A higher value of  $J$  gives a more significant reduction in  $\eta_o$ .
- A slight increase in roughness leads to a large decrease in the value of  $\eta_o$  for the propeller. A large drop in propeller performance can therefore be expected in the early stages of its operation.
- The painting of a propeller is extremely effective. For instance, a propeller coated with foul-release paint had an SSM of 2.7%, while the unpainted propeller required 57.8% extra power with respect to the clean propeller for a period of four years in seawater. Propeller painting using foul-release paint is therefore strongly advised.

Our recommendations for future research work are as follows:

- The propeller model under roughed conditions could be tested in a towing tank.
- The even distribution of roughness considered here could be changed to a non-uniform real distribution, and both experiment and simulation could be conducted.
- A simulation of a full-scale fouled propeller could be a subject for future work, since the size of the roughness cannot be scaled up from a model to a full-scale propeller.
- The model of roughness accumulation is based on an annual roughness increment, whereas measurements at shorter intervals (such as six months) on a full-scale propeller would be very helpful if practically possible.

## NOMENCLATURE

A	Roughness constant	$U_\tau$	Friction velocity
B	Smooth wall log-law intercept	$U^+$	Non-dimensional velocity
$C, C_s$	Roughness constant	$\Delta U^+$	Roughness function
D	Diameter of propeller	$V_s$	Speed of the ship
GCI	Grid convergence index	$V_A$	Propeller advance speed
J	Advance coefficient	w	Wake parameter
$k_s$	Equivalent sand-grain roughness height	$y$	Normal distance from the wall
$k_s^+$	Roughness Reynolds number based on $k_s$	$y^+$	Non-dimensional distance from wall
$K_T$	Thrust coefficient	$\rho$	Fluid density
$K_Q$	Torque coefficient	$\phi_\kappa$	$K_T$ and $K_Q$ on the $k^{th}$ grid
n	Rotational speed of propeller	$\mu$	Dynamic viscosity
$P_B, P_{Bf}$	Engine power (smooth, fouled)	$\kappa$	von Karman constant
$P_D$	Delivered power	$\bar{\tau}_{ij}$	Mean viscous stress tensor components
$P_E$	Effective power	$\eta_D$	Quasi-propulsive efficiency coefficient
$Q, Q_f$	Propeller torque (smooth, fouled)	$\eta_H$	Hull efficiency
$R_a, R_{150}$	Roughness height parameters	$\eta_m$	Mechanical efficiency
$R_T$	Total hull resistance	$\eta_o, \eta_{of}$	Open-water efficiency (smooth, fouled)
SSM	Specific sea margin	$\eta_R$	Relative rotative efficiency
t	Thrust deduction factor	$\nu$	Kinematic viscosity
T	Propeller thrust	$\overline{\rho u_i' u_j'}$	Reynolds stresses
$\overline{u_i}$	Averaged Cartesian component velocity	$U_\tau$	Friction velocity

## REFERENCES

1. IMO, Second IMO GHG Study 2009. London, UK, 2009.
2. A. Banawan, M. Mosleh, and I. Seddiek, "Prediction of the fuel saving and emissions reduction by decreasing speed of a catamaran," J. Mar. Eng. Techno., (3), vol. 12, pp. 40-48, 2013.
3. M. H. Ghaemi and H. Zeraatgar, "Impact of propeller emergence on hull, propeller, engine, and fuel consumption performance in regular waves," Pol. Marit. Res. , (116), vol. 29, pp. 56-76, doi: 10.2478/pomr-2022-0044, 2022.
4. M. Burak Samsul, "Blade cup method for cavitation reduction in marine propellers," Pol. Marit. Res. , 2 (110), vol. 28, pp. 54-62, 10.2478/pomr-2021-0021, 2021.
5. P. Król, "Blade section profile array lifting surface design method for marine screw propeller blade," Pol. Marit. Res. , 4 (1040), vol. 26, pp. 134-141, doi: 10.2478/pomr-2019-0075, 2019.
6. A. Nadery and H. Ghassemi, "Numerical investigation of the hydrodynamic performance of the propeller behind the ship with and without WED," Pol. Marit. Res. , 4 (108), vol. 27, pp. 50-59, doi: 10.2478/pomr-2020-0065, 2020.
7. M. Perić, "Prediction of cavitation on ships," Brodogradnja, vol. 73, no. 3, pp. 39-58, 2022.
8. W. Tarełko, "The effect of hull biofouling on parameters characterizing ship propulsion system efficiency," Pol. Marit. Res. , 4(84), vol. 21, pp. 27-34X, 2014, doi: 10.2478/pomr-2014-0038.

9. L. Guangnian, Q. Chen, and Y. Liu, "Experimental study on dynamic structure of propeller tip vortex," *Pol. Marit. Res.*, 2 (106), vol. 27, pp. 11-18, 2020, doi: 10.2478/pomr-2020-0022.
10. Y. Zhang, X. Wu, M. Lai, G. Zhou, and J. Zhang, "Feasibility study of RANS in predicting propeller cavitation in behind-hull condition," *Pol. Marit. Res.*, 4 (108), vol. 27, pp. 26-35, 2020.
11. ITTC Virtual, The Resistance and Propulsion Committee, Final Report and Recommendations to the 29<sup>th</sup> ITTC, 13-18 June ITTC 2021 Virtual.
12. R. Townsin, and S. Dey, "The correlation of roughness drag with surface characteristics," *Fluid Mechanics and Its Applications*, vol. 6. Springer, Dordrecht, doi: org/10.1007/978-94-011-3526-9\_10, 1991.
13. Y. K. Demirel, "A CFD model for the frictional resistance prediction of antifouling coatings," *Ocean Eng.*, vol. 89, pp. 21-31, 2014.
14. A. Vargas, and H. Shan, "Modeling of ship resistance as a function of biofouling type, coverage, and spatial variation," in *2nd Hull Performance & Insight Conference*, pp. 264-281, Ulrichshusen, Germany, 2017.
15. C. Grigson, "Drag losses of new ships caused by hull finis," *J. Ship Res.*, vol. 36, no. 02, pp. 182-196, 1992.
16. S. Song et al., "Investigating the effect of heterogeneous hull roughness on ship resistance using CFD," *JMSE*, vol. 9, no. 2, p. 1, 2021.
17. T. Cebeci and P. Bradshaw, "Momentum transfer in boundary layers," in *Series in Thermal and Fluids Engineering*, P. Bradshaw, Ed. Washington: Hemisphere Pub. Corp., 1977.
18. A. Farkas, N. Degiuli, and I. Martić, "Towards the prediction of the effect of biofilm on the ship resistance using CFD," *Ocean Eng.*, vol. 167, pp. 169-186, 2018.
19. A. Farkas, N. Degiuli, L. Martic, and R. Dejhalla, "Impact of hard fouling on the ship performance of different ship forms," *JMSE*, vol. 8, p. 748, 2020.
20. A. Farkas, N. Degiuli, and I. Martić, "Impact of biofilm on the resistance characteristics and nominal wake," *Proceedings of the Institution of Mechanical Engineers, Part M: Journal of Engineering for the Maritime Environment*, vol. 234, no. 1, pp. 59-75, 2020.
21. A. Farkas, N. Degiuli, and I. Martić, "A novel method for the determination of frictional resistance coefficient for a plate with inhomogeneous roughness," *Ocean Eng.*, vol. 237, p. 109628, 2021.
22. P. Kellett, K. Mizzi, K. Demirel, and O. Turan, "Investigation the roughness effect of biofouling on propeller performance," *International Conference on Shipping in Changing Climates*, SEMANTIC SCHOLAR, ID 55216316, 2015.
23. D. Owen, Y.K. Demirel, E. Oguz, T. Tezdogan, and A. Incecik, "Investigating the effect of biofouling on propeller characteristics using CFD," *Ocean Eng.*, vol. 159, pp. 505-516, 2018.
24. S. Song, Y. Demirel, and M. Atlar, "An investigation into the effect of biofouling on full-scale propeller performance using CFD," in: *Proceedings of the ASME 2019 38th International Conference on Ocean, Offshore & Arctic Engineering OMAE2019*, June 9-14, 2019, Glasgow, Scotland, UK, 2019.
25. S. Song, Y. Demirel, and M. Atlar, "Propeller performance penalty of biofouling: CFD prediction," *J. Offshore Mech. Arct.*, vol. 142, no. 6, p. 0601901, 2020.
26. A. Farkas, N. Degiuli, and I. Martić, "The impact of biofouling on the propeller performance," *Ocean Eng.*, vol. 219, p. 108376, 2021.
27. A. Farkas, N. Degiuli, and I. Martić, "Assessment of the effect of biofilm on the ship hydrodynamic performance by performance prediction method," *International Journal of Naval Architecture and Ocean Eng.*, vol. 13, pp. 102-114, 2021.
28. A. Farkas, S. Song, N. Degiuli, I. Martić, and Y.K. Demirel, "Impact of biofilm on the ship propulsion characteristics and the speed reduction," *Ocean Eng.*, vol. 199, p. 107033, 2020.
29. M. P. Schultz and K. A. Flack, "The rough-wall turbulent boundary layer from the hydraulically smooth to the fully rough regime," *J. Fluid Mech.*, vol. 580, pp. 381-405, 2007.
30. SVA Hydrodynamic Solutions, "Potsdam Propeller Test Case (PPTC) Open Water Tests with the Model Propeller VP1304," 2011.
31. L. F. Richardson, and J. A. Gaunt, "The deferred approach to the limit," *Philosophical Transactions of the Royal Society of London: Series A*, vol. 226, pp. 299-361, 1927.
32. U. Barkmann, H. Heinke, and L. Lubke, "Potsdam propeller test case (PPTC) test case description," in: *Second International Symposium on Marine Propulsors SMP'11*, Hamburg, Germany, Workshop: Propeller Performance, 2011.



33. M. P. Schultz, "Frictional resistance of antifouling coating systems," J. Fluids Eng., vol. 126, pp. 1039-1047, 2004.

34. J. Carlton, Marine Propellers and Propulsion. London: Butterworth Heinemann, 2010.

## APPENDIX A

### PROPOSED ROUGHNESS FUNCTION MODEL

In this study, the roughness parameters measured by Schultz and Flack [29] are utilised to develop a new roughness function model. The velocity profile on a rough flat plate can be expressed as follows:

$$U^+ = \frac{1}{\kappa} \ln y^+ - \frac{1}{\kappa} \ln k_s^+ + A \quad (\text{A.1})$$

B is added and subtracted:

$$U^+ = \frac{1}{\kappa} \ln y^+ + B - \left( \frac{1}{\kappa} \ln k_s^+ + B - A \right) \quad (\text{A.2})$$

By comparing Eqs. (2) and (A.2),  $\Delta U^+$  can be written as:

$$\Delta U^+ = \frac{1}{\kappa} \ln k_s^+ + B - A \quad (\text{A.3})$$

$C_s$  is introduced as the sand-grain roughness constant, which is defined as follows:

$$\frac{1}{\kappa} \ln C_s = B - A \quad (\text{A.4})$$

Then, Eq. (A.3) can be reparametrized as follows:

$$\Delta U^+ = \frac{1}{\kappa} \ln k_s^+ + \frac{1}{\kappa} \ln C_s = \frac{1}{\kappa} \ln C_s k_s^+ = \frac{1}{\kappa} \ln C k_s^+ \quad (\text{A.5})$$

where  $C$ , the roughness constant, is dependent on the type of roughness of the surface under consideration.

The experiments identified three flow regimes: a hydraulically smooth regime, a transitionally rough regime, and a fully rough regime.

In the rough regime, for a roughness different from the sand-grain, the roughness constant is different. Hence, Eq. (A.5) is applicable to any rough surface, while  $C$  is individually determined.

Schultz and Flack [17] introduced a relation between an engineering surface and an equivalent sand-grain roughness based on the root mean square of the roughness height, skewness, and flatness of the probability density function (pdf). The mean velocity profile is shown in Fig. A.1, and it can be seen that the flow is hydraulically smooth for  $k_s^+ \leq 2.5$  ( $\Delta U^+ = 0$ ). For a higher flow velocity  $k_s^+ \geq 25$ , the flow regime becomes fully rough, and  $\Delta U^+$  will be a linear function of the logarithmic scale of  $k_s^+$ .

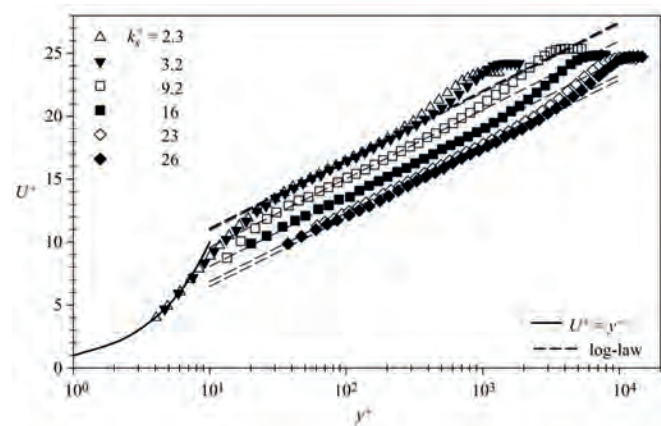


Fig. A.1. Rough wall mean velocity profiles [29].

The roughness constant  $C$  is determined by re-calling Eq. (A.5), as follows:

$$C = \frac{1}{k_s^+} e^{\kappa \Delta U^+} \quad (\text{A.6})$$

Velocity profiles for different surface conditions are shown in Fig. A.1. The downward velocity shift due to roughness in the fully rough regime is 4.6 m/s ( $k_s^+ = 26$ ,  $\Delta U^+ = 4.6$ , and  $\kappa = 0.421$ ). Following Eq. (A.6), the roughness constant  $C$  becomes 0.2667.

The final roughness function model is presented in Eq. (7).